Int. J. Heat Mass Transfer. Vol. 33, No. 5, pp. 815–826, 1990
Printed in Great Britain

0017–9310/90 $3.00 + 0.00

Heat transfer and flow in a radio frequency plasma torch—a new modelling approach

XI CHEN
Department of Engineering Mechanics, Tsinghua University, Beijing 100084, China

(*Received* 18 *March* 1989)

Abstract—A completely two-dimensional (2D) modelling approach including a 2D self-consistent electromagnetic (EM) field formulation is described in this paper to predict the plasma flow and heat transfer in radio frequency (r.f.) plasma torches in which flow and heat transfer are coupled strongly with the EM fields. Computed streamline and temperature contours are presented for different torch power levels and compared with those obtained by the previous approach. Some additional computational results are also given under more complicated heat transfer conditions at the torch wall and concerning the radiative heat flux along the torch wall.

1. INTRODUCTION

SINCE the radio frequency (r.f.) plasma torch was first operated successfully under conditions of atmospheric pressure and flowing gases [1], this type of thermal plasma generator has found a great many applications in inductively coupled plasma (ICP) atomic spectroscopy, the preparation of ultrafine ceramic powders, the rapid pressureless plasma sintering, etc. Along with extensive experimental studies, considerable research efforts have been devoted to the modelling of the r.f. plasma torch, including the earlier one-dimensional (1D) models [2–4] for predicting the temperature distribution at the midsection of the plasma torch coil and various so-called two-dimensional (2D) models for predicting the temperature and flow fields within the whole torch [5–11].

So far the modelling performed by Boulos and his co-workers [6–11] has been accepted as the most sophisticated among the available '2D' models, but this modelling approach is not completely two-dimensional. They solved numerically the 2D continuity, momentum and energy equations, but 1D electromagnetic (EM) field equations were still used. The existence of recirculation vortices within the plasma torch was predicted for the first time by this approach, being qualitatively consistent with previous experimental observations. This modelling approach has also been used to study the influence on the flow and temperature fields in the plasma torch of various different factors such as the type and flow rates of working gases, gas swirling, turbulence, non-LTE (local thermodynamic equilibrium) or two-temperature effect, etc. [7–11]. However, because the 1D EM field formulation in this modelling approach is not satisfactory as shown later on, the present paper will consider the simplest case as discussed in refs. [8, 9], while other complicated factors are left for further studies. For this simplest case, the following assumptions are employed:

(a) 2D (axisymmetrical) flow, temperature and EM fields;

(b) steady and laminar flow without tangential velocity;

(c) LTE and optically thin plasma;

(d) negligible pressure work, viscous dissipation, displacement current and flow-induced electric field.

Under these assumptions, 2D continuity, x- (axial) and r- (radial) momentum and energy equations for the axisymmetrical plasma torch shown in Fig. 1 are given as follows:

$$\frac{\partial}{\partial x}(\rho u)+\frac{1}{r}\frac{\partial}{\partial r}(r\rho v)=0 \tag{1}$$

$$\rho\left(u\frac{\partial u}{\partial x}+v\frac{\partial u}{\partial r}\right)=-\frac{\partial p}{\partial x}+2\frac{\partial}{\partial x}\left(\mu\frac{\partial u}{\partial x}\right)+\frac{1}{r}\frac{\partial}{\partial r}\left[r\mu\left(\frac{\partial u}{\partial r}+\frac{\partial v}{\partial x}\right)\right]+\bar{F}_x-\rho g \tag{2}$$

$$\rho\left(u\frac{\partial v}{\partial x}+v\frac{\partial v}{\partial r}\right)=-\frac{\partial p}{\partial r}+\frac{\partial}{\partial x}\left[\mu\left(\frac{\partial v}{\partial x}+\frac{\partial u}{\partial r}\right)\right]+\frac{2}{r}\frac{\partial}{\partial r}\left(r\mu\frac{\partial v}{\partial r}\right)-2\frac{\mu v}{r^2}+\bar{F}_r \tag{3}$$

$$\rho\left(u\frac{\partial h}{\partial x}+v\frac{\partial h}{\partial r}\right)=\frac{\partial}{\partial x}\left(\frac{\kappa}{C_p}\frac{\partial h}{\partial x}\right)+\frac{1}{r}\frac{\partial}{\partial r}\left(r\frac{\kappa}{C_p}\frac{\partial h}{\partial r}\right)+\bar{q}_3-U_r \tag{4}$$

with the boundary conditions

$$x=0: u=\begin{cases} Q_1/(\pi r_1^2) & \text{as } r<r_1 \\ 0 & \text{as } r_1\leqslant r\leqslant r_2 \\ Q_2/[\pi(r_3^2-r_2^2)] & \text{as } r_2<r<r_3 \\ Q_3/[\pi(R_0^2-r_3^2)] & \text{as } r_3\leqslant r<R_0 \end{cases} \tag{5}$$

$$v=0,\quad h=h_0$$

NOMENCLATURE

- $\mathbf{A}$ vector magnetic potential [V s m^{-1}]
- A_1, A_2 in-phase and out-of-phase amplitudes of A_θ [V s m^{-1}]
- $\mathbf{B}$ magnetic flux density [V s m^{-2}]
- C_p specific heat at constant pressure [J kg^{-1} K^{-1}]
- $\mathbf{E}$ electric field intensity [V m^{-1}]
- $E(k), K(k)$ complete elliptic integrals
- $\mathbf{F}$ Lorentz force, $\mathbf{j} \times \mathbf{B}$ [N m^{-3}]
- g gravity [m s^{-2}]
- h specific enthalpy [J kg^{-1}]
- $\mathbf{H}$ magnetic field strength [A m^{-1}]
- $H_{x\infty}$ factor in equation (13) [A m^{-1}]
- I, I_0 excitation current and its amplitude [A]
- $\mathbf{j}$ conductive current density [A m^{-2}]
- k argument
- L_1, L_2, L lengths in Fig. 1 [m]
- p pressure [N m^{-2}]
- P, P_t temporary and given torch power [W]
- q_w specific heat flux at torch wall [W m^{-2}]
- $\bar{q}_J$ Joule heating power [W m^{-3}]
- Q_1, Q_2, Q_3 volumetric flow rates (Fig. 1) [m^3 s^{-1}]
- Q_{out} energy carried out by plasma flow from torch [W]
- Q_r total radiation power [W]
- Q_w total heat flux to torch wall [W]
- r, R radial coordinate, loop radius [m]
- r_1, r_2, r_3 radii in Fig. 1 [m]
- R_c coil radius [m]
- R_0 torch tube inner radius [m]
- s axial distance between two loops in equation (40) [m]
- t time [s]
- T temperature [K]
- T_{wi}, T_{wo} inner and outer surface temperatures [K]
- u, v axial and radial velocity components [m s^{-1}]
- U_r radiation power per unit volume of plasma [W m^{-3}]
- $\mathbf{V}$ velocity vector [m s^{-1}]
- x axial coordinate.

Greek symbols

- α convective heat transfer coefficient in equation (41) [W m^{-2} K^{-1}]
- δ wall thickness (Fig. 1) [m]
- ε emissivity
- θ azimuthal coordinate
- κ thermal conductivity [W m^{-1} K^{-1}]
- μ viscosity [kg m^{-1} s^{-1}]
- ξ magnetic permeability [H m^{-1}]
- ρ density [kg m^{-3}]
- σ electric conductivity [A V^{-1} m^{-1}]
- σ_0 Stefan–Boltzmann constant [W m^{-2} K^{-4}]
- ϕ, ϕ' angles in Fig. A1
- χ phase angle difference between $\mathbf{H}$ and $\mathbf{E}$
- ω circular frequency [s^{-1}].

Subscripts

- c convective component
- max maximum
- r radial component
- r radiative component
- w torch wall
- x axial position or component
- θ azimuthal component.

Superscript

- $\bar{}$ time-averaged or r.m.s. value.

$$x = L: \quad v = 0, \quad \frac{\partial u}{\partial x} = \frac{\partial h}{\partial x} = 0 \qquad \text{(one-way conditions)} \quad (6)$$

$$r = 0: \quad v = 0, \quad \frac{\partial u}{\partial r} = \frac{\partial h}{\partial r} = 0 \qquad (7)$$

$$r = R_0: \quad u = v = 0, \quad -\left(\frac{\kappa}{C_p}\frac{\partial h}{\partial r}\right)_w = \frac{\kappa_w}{\delta}(T_{wi} - T_{wo}). \qquad (8)$$

$\bar{F}_x$, $\bar{F}_r$ and $\bar{q}_J$ appearing in equations (2)–(4) as source terms are the axial and radial components of the Lorentz force ($\mathbf{j} \times \mathbf{B}$) and the Joule heating power, all time-averaged values. In order to calculate these source terms, one has to solve simultaneously the pertinent EM field equations. On the other hand, since the temperature-dependent electric conductivity of plasma appears in the EM field equations as we see later on, the solution of equations (1)–(4) would couple strongly with the solution of the EM field equations.

Due to the difficulty encountered at that time in solving completely 2D EM field equations, Boulos and his co-workers [6–11], like many previous researchers [2–5], turned to employ a 1D EM field formulation. This EM field formulation has a few drawbacks as we see in the next section. Since a more perfect EM field treatment is highly desirable for the modelling of flow and heat transfer in the r.f. plasma torch, Section 3 describes a new, self-consistent, 2D EM field formulation, which was presented in a recent short communication [12]. Sample predicted results are given for the flow and temperature fields in the r.f.

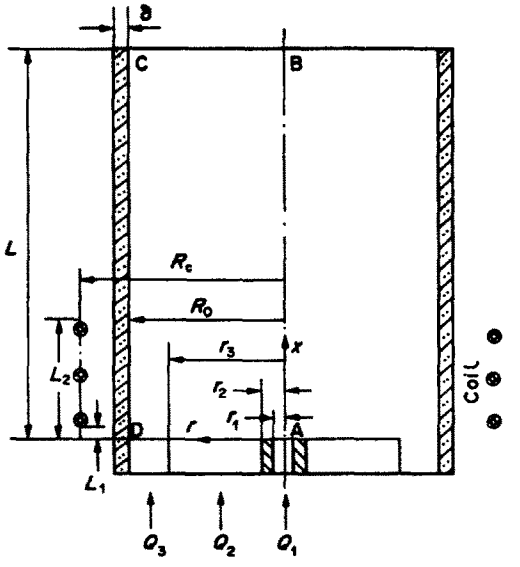

FIG. 1. Schematic diagram of the r.f. plasma torch. $r_1 = 0.0017, r_2 = 0.0037, r_3 = 0.0188, R_0 = 0.025, R_c = 0.033, L_1 = 0.010, L_2 = 0.074, L = 0.25$ and $\delta = 0.002$ (m); $Q_1 = 1$, $Q_2 = 3$ and $Q_3 = 16$ (ST litres min^{-1}); $T_{w_0} = 350$ K; frequency 3 MHz; 1 atm argon.

plasma torch shown in Fig. 1 and compared with their counterparts obtained by the previous approach in Section 4.

2. DRAWBACKS OF THE PREVIOUS EM FIELD FORMULATION

In order to simplify the calculation of the EM fields in an axisymmetrical r.f. plasma torch, Boulos and co-workers [6–11] in their modelling approach assumed that the magnetic field had only an axial component, i.e. $\mathbf{H} = (0, 0, \bar{H}_x)$ in cylindrical coordinates (r, θ, x), besides the electric field had only a θ-component, i.e. $\mathbf{E} = (0, \bar{E}_\theta, 0)$. The r.m.s. values of the electric and magnetic fields were calculated by solving the following first-order ordinary differential equations:

$$\frac{1}{r}\frac{\mathrm{d}}{\mathrm{d}r}(r\bar{E}_\theta) = -\xi\omega\bar{H}_x \sin\chi \tag{9}$$

$$\frac{\mathrm{d}\bar{H}_x}{\mathrm{d}r} = -\sigma\bar{E}_\theta \cos\chi \tag{10}$$

$$\frac{\mathrm{d}\chi}{\mathrm{d}r} = (\sigma\bar{E}_\theta/\bar{H}_x)\sin\chi - (\xi\omega\bar{H}_x/\bar{E}_\theta)\cos\chi \tag{11}$$

with the boundary conditions: along the torch axis $(r = 0)$

$$\bar{E}_\theta = 0 \tag{12}$$

$$\bar{H}_x = H_{x\infty}\left\{\frac{L_2 - x}{[R_c^2 + (L_2 - x)^2]^{1/2}} - \frac{L_1 - x}{[R_c^2 + (L_1 - x)^2]^{1/2}}\right\} \tag{13}$$

$$\chi = \frac{\pi}{2}. \tag{14}$$

Correspondingly, the axial component of the Lorentz force $\bar{F}_x$ in equation (2) would be zero, while the radial component of the force is

$$\bar{F}_r = \sigma\xi\bar{E}_\theta\bar{H}_x \cos\chi. \tag{15}$$†

The time averaged Joule heating power is

$$\bar{q}_J = \sigma\bar{E}_\theta^2. \tag{16}$$

In equations (9)–(11) χ is the phase angle difference between the local electric and magnetic fields. Due to the presence of the induction electric current in the plasma, χ would vary with the position within the plasma torch and is determined by equation (11).

Equations (9)–(11) and their boundary conditions were initially proposed in ref. [13], and only a minor amendment in signs was adopted in refs. [7–11]. However, there still exists a drawback in the formulation presented above. Namely, calculated results show that the r.m.s. value of the electric field, $\bar{E}_\theta$, is always negative or zero within the whole torch, and thus is obviously unreasonable. This drawback is not critical since it does not affect the calculated results of the flow and temperature fields in the torch and can be amended easily by using $\chi = -\pi/2$ instead of $\chi = \pi/2$ in boundary condition (14).

A more important drawback of the available EM field formulation is associated with the assumption that the magnetic field has only an axial component and with the use of boundary condition (13). The radial component of the magnetic field cannot be completely neglected in comparison with its axial component for actual r.f. plasma torches in which the excitation coil usually consists of few turns and the length/diameter ratio of the coil is usually not large. Equation (13) is similar to the well-known expression for the axial magnetic field distribution along the axis of a solenoid with finite length in free space. Equation (13) was adopted in refs. [6–11] in order to include the variation of H_x with x. It was assumed in refs. [6–11] that the effect of the presence of plasma on the axial magnetic field within the torch was represented only by the proportional reduction of the factor $H_{x\infty}$, but this assumption did not agree with available experimental observation [10]. Moreover, such an EM field formulation would violate at least one of Maxwell's equations. Because it was assumed that the magnetic field had only an axial component, one of Maxwell's equations, $\nabla \cdot \mathbf{B} = 0$, would require $\partial H_x/\partial x = 0$. Boundary condition (13) does not obviously satisfy this requirement. Hence, the available EM field formulation is not self-consistent. This drawback is also shared by Yoshida *et al.* [14]. They also assumed a 1D magnetic field (axial) and employed an

† A minus sign was used on the right-hand side in refs. [6–11], but it is obviously an error.

x-dependent magnetic field as a boundary condition, although a somewhat different magnetic field equation was solved in ref. [14].

3. A NEW MODELLING APPROACH INCLUDING SELF-CONSISTENT 2D EM FIELD FORMULATION

In this approach, equations (1)–(4) and their boundary conditions (5)–(8) are still employed for the calculation of the flow and temperature fields in r.f. plasma torches, but a completely 2D EM field formulation will be used due to the drawbacks of the previous approach as indicated above.

For the case in question in which the displacement current and the plasma-flow-induced field ($\mathbf{V}\times\mathbf{B}$) are negligible, Maxwell's equations reduce to

$$\nabla\cdot\mathbf{E}=0 \tag{17}$$

$$\nabla\cdot\mathbf{B}=0 \tag{18}$$

$$\nabla\times\mathbf{E}=-\frac{\partial\mathbf{B}}{\partial t} \tag{19}$$

$$\nabla\times\mathbf{B}=\xi\mathbf{j} \tag{20}$$

and Ohm's law becomes

$$\mathbf{j}=\sigma\mathbf{E}. \tag{21}$$

As we introduce the vector potential $\mathbf{A}$ which satisfies $\mathbf{B}=\nabla\times\mathbf{A}$, equation (18) would be automatically satisfied. We further employ the Coulomb convention $\nabla\cdot\mathbf{A}=0$ [15] and neglect any electrostatic field [16], then the following relations would be obtained from equations (17), (19) and (20):

$$\nabla^2\mathbf{A}=-\xi\mathbf{j} \tag{22}$$

$$\mathbf{E}=-\frac{\partial\mathbf{A}}{\partial t}. \tag{23}$$

For an axisymmetrical r.f. plasma torch in question, the imposing current flowing through the excitation coil of the plasma torch has been assumed to be only an azimuthal component. As a result, the vector potential $\mathbf{A}$, the electric field $\mathbf{E}$ and the conductive current within the plasma $\mathbf{j}$ would all have only azimuthal components in the whole plasma torch, and equations (21)–(23) reduce to

$$j_\theta=\sigma E_\theta \tag{24}$$

$$\frac{1}{r}\frac{\partial}{\partial r}\left(r\frac{\partial A_\theta}{\partial r}\right)+\frac{\partial^2 A_\theta}{\partial x^2}-\frac{A_\theta}{r^2}=-\xi j_\theta \tag{25}$$

$$E_\theta=-\frac{\partial A_\theta}{\partial t}. \tag{26}$$

If we express the r.f. excitation current flowing through the torch coil as

$$I=I_0\cos(\omega t) \tag{27}$$

in which I_0 is the amplitude of the excitation current, A_θ would include both in-phase and out-of-phase components with respect to the excitation current I due to the presence of the induction current in the plasma j_θ and could be expressed as

$$A_\theta=A_1\cos(\omega t)+A_2\sin(\omega t) \tag{28}$$

where A_1 and A_2 are the amplitudes of the in-phase and out-of-phase components of A_θ, respectively. Correspondingly, we have

$$E_\theta=\omega[A_1\sin(\omega t)-A_2\cos(\omega t)] \tag{29}$$

$$B_r=-\frac{\partial A_1}{\partial x}\cos(\omega t)-\frac{\partial A_2}{\partial x}\sin(\omega t) \tag{30}$$

$$B_x=\frac{1}{r}\frac{\partial}{\partial r}(rA_1)\cos(\omega t)+\frac{1}{r}\frac{\partial}{\partial r}(rA_2)\sin(\omega t). \tag{31}$$

Substituting equation (29) into equation (24) and then into equation (25), we obtain the governing equations for the in-phase and out-of-phase amplitudes as follows:

$$\frac{1}{r}\frac{\partial}{\partial r}\left(r\frac{\partial A_1}{\partial r}\right)+\frac{\partial^2 A_1}{\partial x^2}-\frac{A_1}{r^2}-\sigma\xi\omega A_2=0 \tag{32}$$

$$\frac{1}{r}\frac{\partial}{\partial r}\left(r\frac{\partial A_2}{\partial r}\right)+\frac{\partial^2 A_2}{\partial x^2}-\frac{A_2}{r^2}+\sigma\xi\omega A_1=0. \tag{33}$$

The radial and axial components of the Lorentz force ($\bar{F}_r$ and $\bar{F}_x$) and the Joule heating rate ($\bar{q}_j$) appearing as source terms in equations (2)–(4) can then be expressed by A_1 and A_2 as

$$\bar{F}_r=\frac{\sigma\omega}{2r}\left[A_1\frac{\partial}{\partial r}(rA_2)-A_2\frac{\partial}{\partial r}(rA_1)\right] \tag{34}$$

$$\bar{F}_x=\frac{\sigma\omega}{2}\left[A_1\left(\frac{\partial A_2}{\partial x}\right)-A_2\left(\frac{\partial A_1}{\partial x}\right)\right] \tag{35}$$

$$\bar{q}_j=\frac{\sigma\omega^2}{2}(A_1^2+A_2^2) \tag{36}$$

after taking the average over a period of r.f. oscillation.

Equations (32) and (33) are the required 2D EM field equations to be simultaneously solved with equations (1)–(4) in order to determine the flow and temperature fields in r.f. plasma torches. The main difficulty in solving equations (32) and (33) is associated with the specification of their boundary conditions. Although the following boundary conditions can be used:

$$r=0\ \text{(torch axis)}:\quad A_1=A_2=0 \tag{37}$$

$$r\to\infty\quad\text{and}\quad x\to\pm\infty\ \text{(far away)}:\quad A_1=A_2=0 \tag{38}$$

using condition (38) would be extremely inconvenient in a practical computation since it needs to use a much larger computational domain for equations (32) and (33) than that for equations (1)–(4). Hence, we turn

to another approach, i.e. using a common computational domain, A–B–C–D–A (Fig. 1), for the solution of both sets of equations, equations (1)–(4) and equations (32) and (33). The new problem is how to determine the boundary conditions of A_1 and A_2 at the B–C, C–D and A–D boundaries (A_1 and A_2 values along the A–B boundary are given by equation (37)), since the A_1 and A_2 values at these boundaries are not accurately known at the beginning. In this study, those unknown A_1 and A_2 boundary values are determined in the iteration process of solving equations (1)–(4), (32) and (33). Starting the computation from a guessed spatial distribution of A_1 and A_2, we can obtain the corresponding distribution of the induction current j_θ in the plasma. A_1 and A_2 values at boundaries B–C, C–D and A–D are then determined by summing the contribution to A_1 and A_2 of both the excitation current (only to A_1) and the induction currents (to both A_1 and A_2) by using the following A_θ formula of a single current-carrying circular loop for each current [15]:

$$A_\theta = \frac{\xi I_\theta}{2\pi}\sqrt{\left(\frac{R}{r}\right)}\left[\left(\frac{2}{k}-k\right)K(k)-\frac{2}{k}E(k)\right] \quad (39)$$

where $K(k)$ and $E(k)$ are the complete elliptic integrals of the first and second kinds, respectively, and can be readily calculated by using their polynomial approximations given in ref. [15]. I_θ is equal to I for the excitation current in the torch coil (only with the cos ωt component) or equal to $j_\theta \Delta r \Delta x$ for the induction currents within the plasma (with both cos ωt and sin ωt components). The argument in $K(k)$ and $E(k)$ is defined as [15]

$$k = 2\sqrt{\left(\frac{Rr}{(R+r)^2+s^2}\right)} \quad (40)$$

in which R is the radius of the single current-carrying circular loop under consideration; r the radius of the boundary point where A_θ is to be calculated; and s the axial distance between the current-carrying circular loop and the boundary point. The boundary values of A_1 and A_2 should be calculated by including all the coil turns with excitation current I (three turns for the plasma torch in Fig. 1) and all the elementary areas with the induction current $j_\theta \Delta r \Delta x$ in the whole computational domain.

Using the A_1 and A_2 boundary values to solve equations (32) and (33), we obtain new A_1 and A_2 distributions and thus the A_1 and A_2 boundary conditions can be renewed after the j_θ distribution is calculated. Repeating this iteration process until convergence, the correct A_1 and A_2 boundary conditions and their spatial distributions are finally obtained. $\bar{F}_x$, $\bar{F}_r$ and $\bar{q}_j$ calculated in each iteration by using equations (34)–(36) are employed to solve equations (1)–(4).

Equations (1)–(4), (32) and (33) are simultaneously solved using the finite-difference method described by Patankar [17], only the SIMPLEC algorithm [18] has been employed in order to speed convergence. As in ref. [9], 22×17 grid points (nonuniform) and actual temperature-dependent LTE properties (ρ, μ, κ, h, C_p, σ and U_r) of argon plasma at atmospheric pressure are used in this study. It is found that a convergent solution can be obtained for the flow, temperature and EM fields, provided that proper relaxation factors (1.0 for pressure, 0.5–0.7 for others) and appropriate initially guessed fields are employed. However, many more iterations are required than those for the case using the previous approach [9] in order to obtain a convergent solution due to the continuous variation of the boundary conditions of equations (32) and (33) in the iteration process.

For a given torch power (e.g. 7 kW), the iteration solution of equations (1)–(4), (32) and (33) starts from a guessed value of the excitation current, I_0, and the I_0 value is modified in the iteration process as follows: at the end of each round iteration, the torch power is calculated by

$$P = \int_0^L \int_0^{R_0} \bar{q}_j \, 2\pi r \, dr \, dx$$

$$= \int_0^L \int_0^{R_0} \frac{\sigma\omega^2}{2}(A_1^2 + A_2^2) \, 2\pi r \, dr \, dx.$$

In general, the calculated power P is not equal to the given power P_t. The factor $\sqrt{(P_t/P)}$ is used to modify the amplitude value of the excitation current I_θ and A_1 and A_2 distributions. An under-relaxation is also used in order to avoid divergence.

4. RESULTS AND DISCUSSION

For the sake of comparison with the previous approach [8, 9], computational studies are conducted for a typical r.f. plasma torch studied in ref. [8] which is shown in Fig. 1. The frequency of the plasma torch is 3 MHz, while other parameters are shown in Fig. 1. Figures 2–5 show respectively the computed streamline (left half) and temperature (right half) contours at four different torch power levels by the present and the previous approaches. As shown in Fig. 2, for this case with higher power (7 kW), both approaches obtain similar flow and temperature fields. Namely, they all obtain two recirculation vortices in the computed flow field, one being near the torch inlet and extends to the torch axis and another being located near the rear end of the torch coil and near the torch wall. They all show off-axis highest temperature regions due to the presence of skin effect in the plasma. However, the size and the strength of the recirculation vortices in the flow field predicted by the present approach are appreciably smaller than their counterparts obtained by the previous approach [8, 9]. There is also a difference between the two approaches in the predicted temperature fields, especially within the coil region. Almost the same conclusions can be obtained

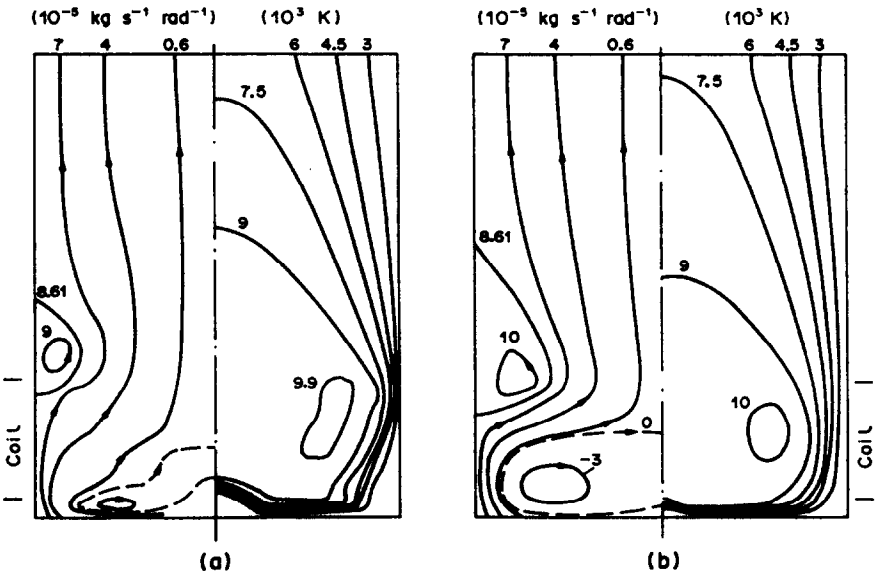

FIG. 2. Computed streamline (left half) and temperature (right half) contours by the present (a) and the previous (b) approaches. Torch power 7 kW.

for the 5 kW (Fig. 3) and 3 kW (Fig. 4) torches, although the shoulder recirculation vortex near the end of the plasma coil reduces in size with decreasing torch power. However, a pronounced difference is found between the predicted flow and temperature fields by the two approaches for a 1 kW plasma torch, as seen in Fig. 5. For this case with lower torch power, the two approaches predict quite different EM fields and, thus, different Lorentz force and Joule heating power distributions. Figure 6 compares the computed Lorentz force distributions obtained by the present and the previous approaches. $\bar{F}_r$ distributions in Fig. 6(a) show that the two approaches predict different form and maximum-value position of the $\bar{F}_r$ contours. The previous approach [6–11] constricts the EM field calculation within the coil region, ignoring any EM fields outside the coil region. The predicted results by the present approach demonstrate that this 1D EM field treatment is too simple to represent the actual EM fields so that the EM fields and Lorentz force distributions cannot be correctly predicted. Since the previous 1D EM field formulation assumed that **B** had only its axial component, the axial component of the Lorentz force, $\bar{F}_x$, was always equal to zero.

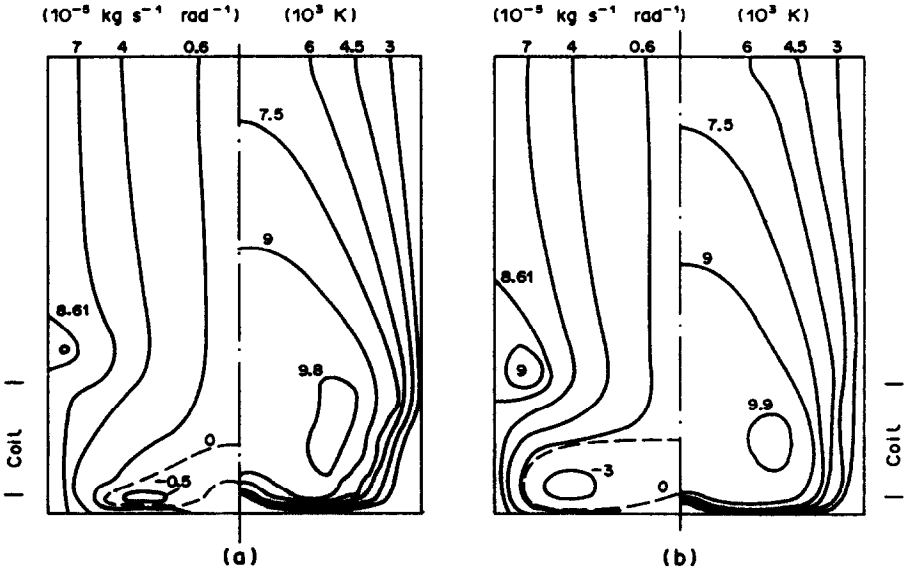

FIG. 3. Computed streamline (left half) and temperature (right half) contours by the present (a) and the previous (b) approaches. Torch power 5 kW.

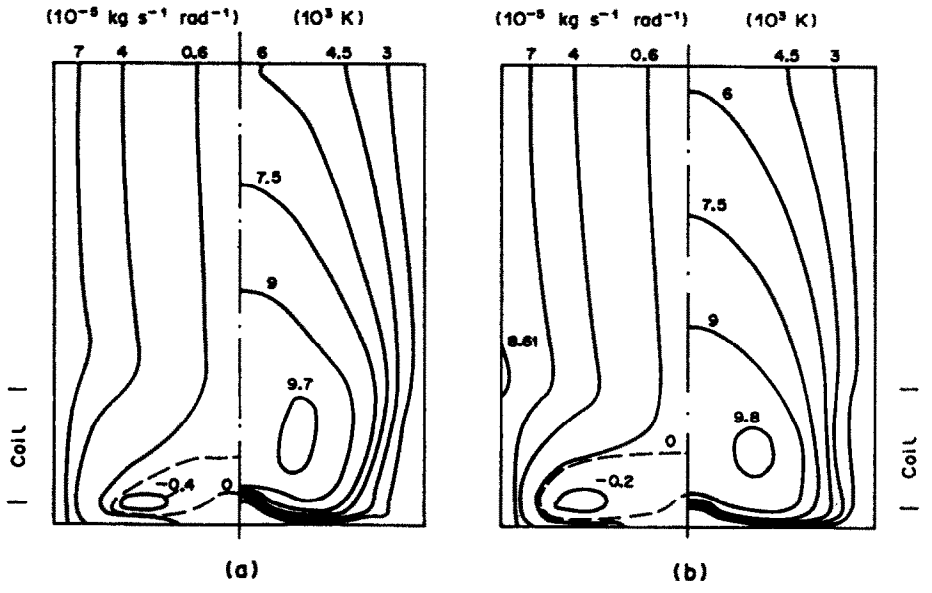

FIG. 4. Computed streamline (left half) and temperature (right half) contours by the present (a) and the previous (b) approaches. Torch power 3 kW.

However, the present 2D EM field formulation predicts that although $\bar{F}_x$ is smaller than $\bar{F}_r$ in their maximums, $\bar{F}_x$ is not negligible in comparison with $\bar{F}_r$, especially within the coil region. Figure 6(b) shows that $\bar{F}_x$ is positive (accelerates flow) within the coil region but it has a negative sign (decelerates flow) in the whole downstream region of the torch. Both $\bar{F}_r$ and $\bar{F}_x$ decrease rapidly with axial distance from the rear end of the torch coil, but they cannot be neglected in the region near the coil. Figure 7 compares the Joule-heating-power density distributions predicted by the two approaches. A pronounced difference between the predicted results is also revealed.

Figures 8(a) and (b) compare the axial velocity and temperature variations along the torch axis by the previous and the present approaches for two different torch powers (1 and 7 kW), respectively. For the torch with higher power (7 kW), the two approaches predict almost the same temperature distributions along the torch axis except near the torch inlet, but different axial velocity variations along the torch axis. Maximum values of both forward and reverse flow

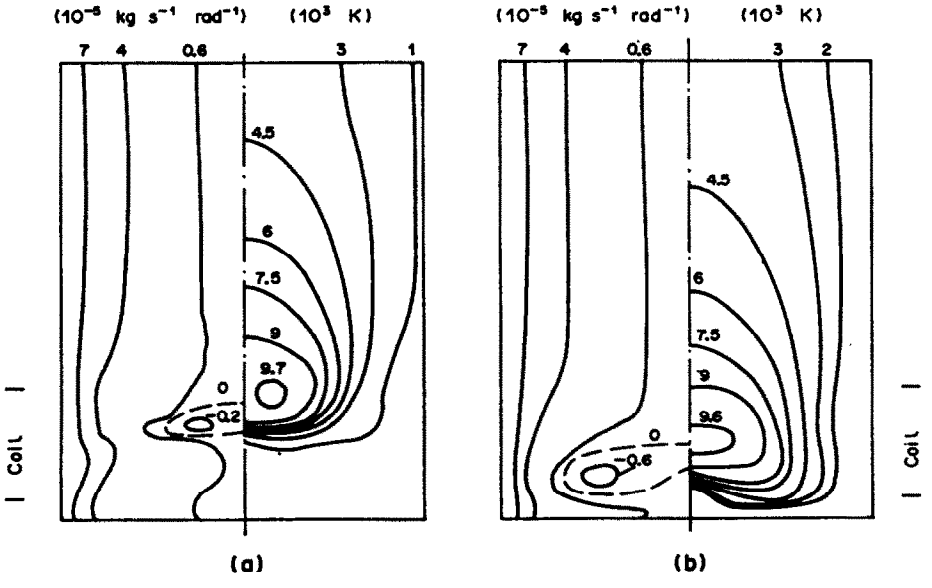

FIG. 5. Computed streamline (left half) and temperature (right half) contours by the present (a) and the previous (b) approaches. Torch power 1 kW.

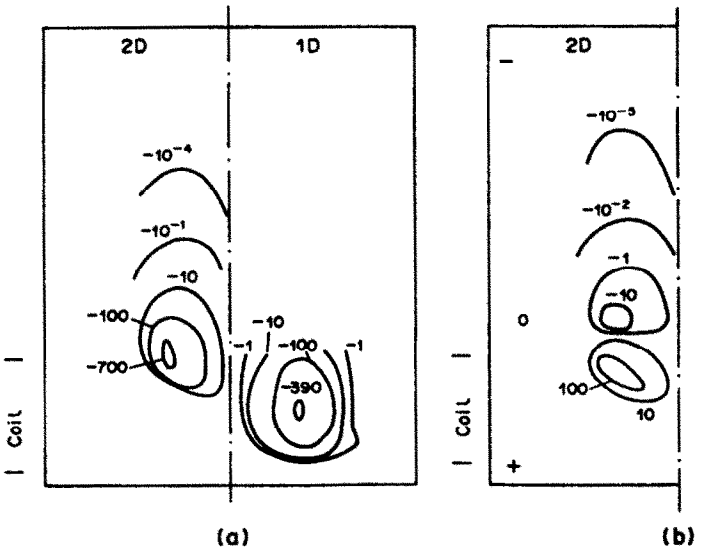

FIG. 6. Computed Lorentz force component contours: (a) radial component $\bar{F}_r$ by the present (2D) and the previous (1D) approaches; (b) axial component $\bar{F}_x$ by the present approach. Torch power 1 kW.

velocities predicted by the present approach are appreciably less than their counterparts by the previous approach. On the other hand, for the torch with lower power (1 kW), a pronounced difference exists between the present and the previous approaches in both temperature and axial velocity variations along the torch axis.

In brief, this study shows that the previous approach based on 1D EM field formulation cannot guarantee the correct flow and temperature field to be predicted. It is recommended that the present self-

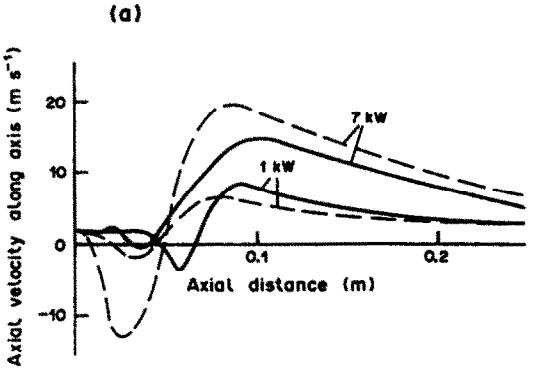

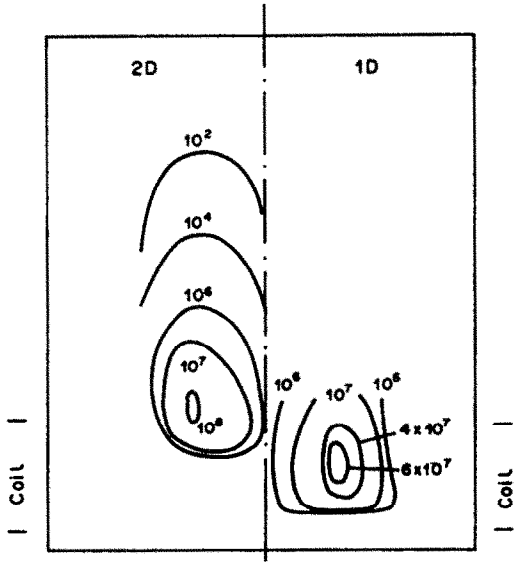

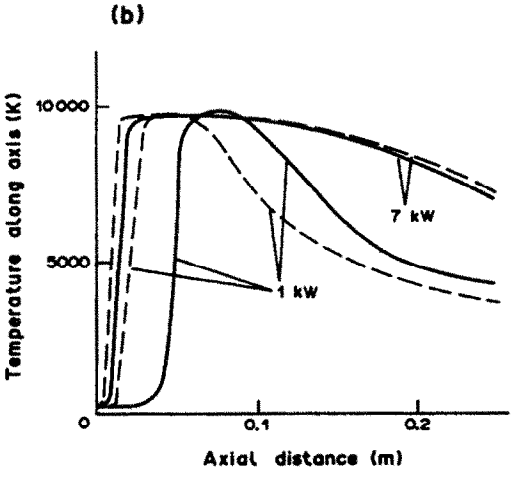

FIG. 7. Comparison of the computed Joule heating rate distributions by the present (2D) and the previous (1D) approaches. Torch power 1 kW.

FIG. 8. Computed axial velocity (a) and temperature (b) distributions along the torch axis by the present (——) and the previous (– – – –) approaches for 1 and 7 kW torches.

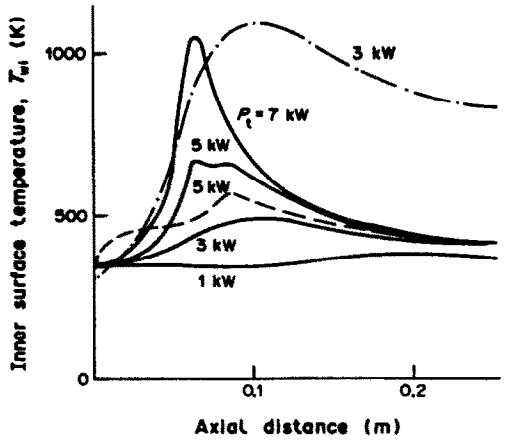

FIG. 9. Computed temperature distributions along the inner surface of a quartz tube wall: ——, by the present approach for 7, 5, 3 and 1 kW torches with T_{wo} = 350 K; – – – –, by the previous approach for a 5 kW torch; — · — · —, by the present approach for a 3 kW torch but using heat transfer boundary condition (41).

consistent 2D EM field formulation should be employed to couple with the 2D continuity, momentum and energy equations in further modelling works of plasma flow and heat transfer within r.f. plasma torches.

Figure 9 shows the computed temperature distributions along the inner surface of the torch wall for different torch power levels. Since the outer surface temperature of the torch wall is taken as 350 K and the wall heat flux is proportional to the temperature difference between the inner and outer surfaces, the T_{wi} distributions in Fig. 9 also reflect the heat flux distributions along the inner surface of the torch wall at corresponding torch power levels. As expected, the highest wall temperature increases with increasing torch power. Figure 9 also shows a temperature distribution along the inner wall surface obtained by the previous approach [8, 9] for a 5 kW plasma torch. The difference between the predicted wall temperatures by the two approaches is appreciable.

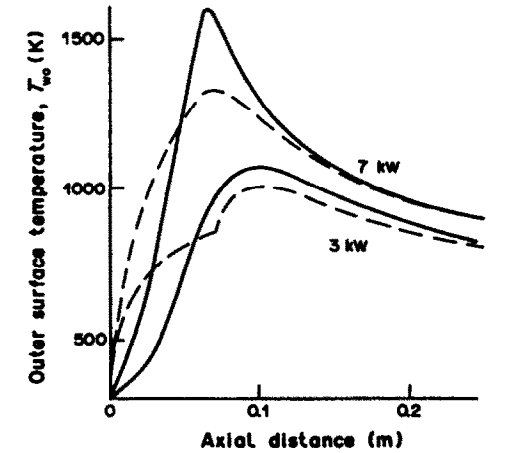

FIG. 10. Computed temperature distributions along the outer surface of a quartz tube (κ_w = 6 W m^{-1} K^{-1}) for 7 and 3 kW torches with the naturally cooled boundary condition (41): ——, by the present approach; – – – –, by the previous approach.

Predicted results by the present approach for some typical torch parameters are collected in Table 1 for different torch power levels, including the total heat flux to the torch wall (Q_w), the power carried out by the effluent plasma from the torch (Q_{out}), the total radiation power (Q_r), the maximum values of radial and axial Lorentz forces ($(-\bar{F}_r)_{max}$ and $\bar{F}_{x,max}$), the highest temperature and axial velocity (T_{max} and u_{max}), and the amplitude of the excitation current flowing through the torch coil (I_0). It is seen from Table 1 that as the torch power is enhanced from 3 to 5 kW and then to 7 kW, Q_{out} increases only slightly while Q_w and Q_r increase rapidly. Hence, enhancing torch power is not a good method to increase the heating efficiency of the working gas. This point is even more easily obtained by examining the fraction of Q_w, Q_{out} and Q_r in the total torch power (P_t): with the increase of the torch power, Q_{out}/P_t reduces rapidly, Q_r/P_t increases appreciably, while Q_w/P_t remains almost unchanged. The reason for this phenomenon to appear is that the increase of the torch power is associated with the rapid enlargement of the high-temperature 'fire-ball' region while T_{max} remains almost a constant. This fact results in a rapid increase of the heat losses Q_w and Q_r, while Q_{out} increases only slightly. All the other parameters including $(-\bar{F}_r)_{max}$, $(\bar{F}_x)_{max}$, u_{max} and I_0 are enhanced appreciably with the increase of the torch power. However, Table 1 shows that the 1 kW torch seems to be quite different from the other higher power torches. This lower power torch gives rather high heating efficiency of the working gas (Q_{out}/P_t = 68%) and much lower wall heat flux and radiation power. It is for this 1 kW torch that a pronounced difference between the predicted flow and temperature fields by the present and the previous approaches is found, as mentioned above.

All the foregoing computation is concerned with the heat transfer boundary condition at the torch tube (quartz tube) that the outer surface temperature of the quartz tube is fixed at 350 K. A plasma torch with a water-cooled outer surface of the torch tube would correspond approximately to this case. Additional computational studies are also conducted for the case of naturally cooled plasma torches. Namely, the outer surface of the plasma torch is cooled by both the natural convection and thermal radiation in the 300 K surroundings

$$q_w = \kappa_w(T_{wi} - T_{wo})/\delta = \alpha(T_{wo} - T_\infty) + \varepsilon\sigma_0(T_{wo}^4 - T_\infty^4). \quad (41)$$

The convective heat transfer coefficient α is calculated by using the well-known correlation for the naturally convective heat transfer between a horizontal cylinder and the ambient air at 300 K. σ_0 is the Stefan–Boltzmann constant, while ε is the emissivity of the torch

Table 1. Torch parameters for four different plasma torch powers obtained by the present modelling approach

Torch power, P_t (W)	1000	3000	5000	7000
Coil current, I_0 (A)	193	125	145	163
Wall heat flux, Q_w (W)	314	1741	3030	4170
Q_w/P_t	0.314	0.580	0.607	0.596
Radiation heat flux, Q_r (W)	27	216	764	1560
Q_r/P_t	0.027	0.072	0.153	0.223
Plasma flow energy, Q_{out} (W)	684	1048	1200	1270
Q_{out}/P_t	0.684	0.349	0.240	0.181
Radial Lorentz force, $(-\bar{F}_r)_{max}$ (N m^{-3})	751	580	939	1330
Axial Lorentz force $(\bar{F}_x)_{max}$ (N m^{-3})	191	63.5	168	252
Temperature, T_{max} (K)	9750	9750	9860	9970
Axial velocity, $(u_x)_{max}$ (m s^{-1})	8.31	10.8	13.1	14.6

wall (quartz) and is taken as 1.0 in the computation for simplicity. Computed temperature distributions along the outer surface of the plasma torch by the present and the previous approaches are shown in Fig. 10 for two torch powers (3 and 7 kW). The highest value of the outer surface temperature along the torch wall increases with increasing torch power. The previous approach [8, 9] predicts somewhat lower values for the highest outer surface temperature, as one can see in Fig. 10. Since T_{wo} may assume much higher values than 350 K under conditions of naturally cooled plasma torches, the inner surface temperatures, T_{wi}, are also much higher than their counterparts for water-cooled plasma torches as a sample calculated result shown in Fig. 9 demonstrates.

Only the convective heat flux from the plasma to the torch wall is considered in the foregoing wall temperature calculations since little is known about how much radiation heat flux is absorbed by the torch inner surface or by the quartz wall itself. The radiative heat flux incident to the inner surface of the plasma torch at position (x, R_0) can be calculated by using the following relation (see Appendix):

$$(q_{w,r})_x = \sum_{i,j} \frac{U_t r_j \Delta x_i \Delta r_j}{2\pi R_0^2} \times \int_0^{\pi} \frac{[1-(r_j/R_0)\cos\theta]\,d\theta}{\{1+(r_j/R_0)^2+[(x-x_i)/R_0]^2-2(r_j/R_0)\cos\theta\}^{3/2}}. \quad (42)$$

The summation in equation (42) should include all the elementary areas in the computational domain which have a contribution to the radiative heat flux. Calculated results of both the convective and radiative heat fluxes by the present and the previous approaches are compared in Figs. 11(a) and (b) for the 7 and 3 kW plasma torches, respectively. An appreciable difference exists between the predicted results by the two approaches for both the convective and radiative heat fluxes and for both the 7 and 3 kW torches. For example, for the 7 kW plasma torch, the present approach predicts that the maximum convection heat flux, $(q_{w,c})_{max}$, is much higher than the maximum radiation heat flux, $(q_{w,r})_{max}$, while a different prediction is given by the previous approach [8, 9]. In general, the present approach predicts a higher $(q_{w,c})_{max}$ but a lower $(q_{w,r})_{max}$ than those given by the previous approach.

5. CONCLUSIONS

The 1D EM field formulation employed to calculate the Lorentz force and Joule heating terms in the momentum and energy equations is not self-consis-

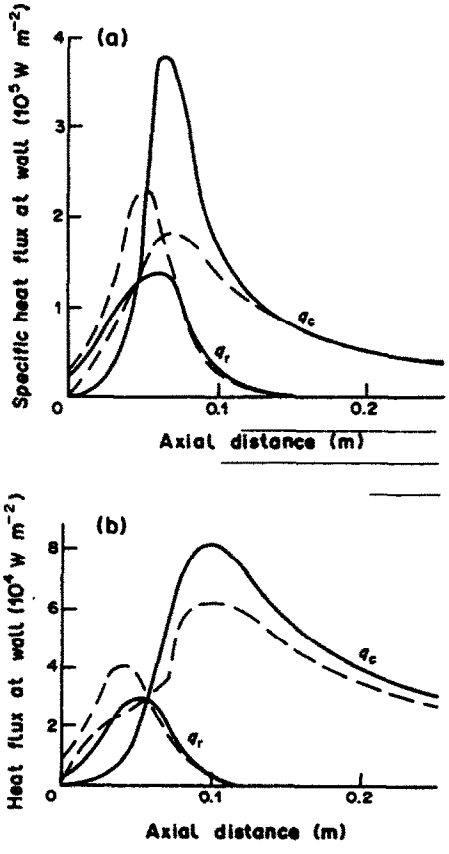

FIG. 11. Comparison of the computed heat flux distributions along the torch wall of the convective (q_c) and radiative (q_r) heat transfer by the present (——) and by the previous (– – – –) approaches for 7 kW (a) and 3 kW (b) torches.

tent, so that the plasma flow and heat transfer cannot be accurately predicted by the previous '2D' modelling approach [6–11]. An improved, self-consistent, completely 2D EM field formulation is employed in this paper to couple with 2D continuity, momentum and energy equations for predicting the flow and temperature fields in the r.f. plasma torch. Sample calculation results for several different torch power levels are presented and compared with those obtained by the previous approach, showing that the present modelling approach should be used in further studies. Additional calculated results are also given concerning the radiative heat flux along the inner surface of the plasma torch wall and for the case with more complicated heat transfer boundary conditions.

Acknowledgement—This work was supported by the National Natural Science Foundation of China.

REFERENCES

1. T. B. Reed, Induction-coupled plasma torch, *J. Appl. Phys.* **32**, 821–824 (1961).
2. M. P. Freeman and J. D. Chase, Energy-transfer mechanism and typical operating characteristics for the rf plasma generator, *J. Appl. Phys.* **39**, 180–190 (1968).
3. H. U. Eckert, Analysis of thermal induction plasmas dominated by radial conduction losses, *J. Appl. Phys.* **41**, 1520–1528 (1970).
4. H. U. Eckert, Analytical treatment of radiation and conduction losses in thermal induction plasmas, *J. Appl. Phys.* **41**, 1529–1537 (1970).
5. R. C. Miller and R. J. Ayen, Temperature profiles and energy balances for an inductively coupled plasma torch, *J. Appl. Phys.* **40**, 5260–5273 (1969).
6. M. I. Boulos, Flow and temperature fields in the fireball of an inductively coupled plasma, *IEEE Trans. Plasma Sci.* **PS-6**, 28–39 (1976).
7. M. I. Boulos, R. Gagne and R. M. Barnes, Effect of swirl and confinement on the flow and temperature fields in an inductively coupled r.f. plasma, *Can. J. Chem. Engng* **58**, 367–381 (1980).
8. J. Mostaghimi, P. Proulx and M. I. Boulos, Parametric study of the flow and temperature fields in an inductively coupled r.f. plasma torch, *Plasma Chem. Plasma Process.* **4**, 199–217 (1984).
9. J. Mostaghimi, P. Proulx and M. I. Boulos, An analysis of the computer modeling of the flow and temperature fields in an inductively coupled plasma, *Numer. Heat Transfer* **8**, 187–201 (1985).
10. M. I. Boulos, The inductively coupled R.F. (radio frequency) plasma, *Pure Appl. Chem.* **57**, 1321–1352 (1985).
11. J. Mostaghimi, P. Proulx and M. I. Boulos, A two-temperature model of the inductively coupled r.f. plasma, *J. Appl. Phys.* **61**, 1754–1760 (1987).
12. Xi Chen, Modeling of a radio-frequency plasma torch including a self-consistent electromagnetic field formulation, *J. Phys. D: Appl. Phys.* **22**, 361–363 (1989).
13. A. E. Mensing and L. R. Boedeker, Theoretical investigations of R.F. induction heated plasma, NASA Contract Report CR-1312 (1969).
14. T. Yoshida, K. Nakagawa, T. Harada and K. Akashi, New design of a radio-frequency plasma torch, *Plasma Chem. Plasma Process.* **1**, 113–129 (1981).
15. P. Silvester, *Modern Electromagnetic Fields*, pp. 143–156, 320. Prentice-Hall, Englewood Cliffs, New Jersey (1968).
16. N. Contaxes and A. J. Hatch, High-frequency fields in solenoidal coils, *J. Appl. Phys.* **40**, 3548–3550 (1969).
17. S. V. Patankar, *Numerical Heat Transfer and Fluid Flow*. Hemisphere, Washington, DC (1980).
18. J. P. Van Doormaal and G. D. Raithby, Enhancements of the SIMPLE method for predicting incompressible fluid flows, *Numer. Heat Transfer* **7**, 147–163 (1984).
19. B. D. Hunn and R. J. Moffat, Radiative heat transfer from a plasma in tube flow, *Int. J. Heat Mass Transfer* **17**, 1319–1328 (1974).

APPENDIX

The angle factor for the radiation energy leaving the elementary gas volume $r_j\,dr\,d\theta\,dx$ around point P (Fig. A1) with coordinates (r_j, θ', x_i) to an elementary area on the plasma torch wall $R_0\,d\theta\,dx$ around the point (R_0, θ, x) is

$$\frac{R_0\,d\theta\,dx}{4\pi s_d^2}\cos\phi\sin\phi'. \tag{A1}$$

Noting $s_d^2 = d^2+s^2$, $\cos\phi = (R_0-r_j\cos\theta)/d$, $\sin\phi' = d/s_d$ (see Fig. A1), (A1) becomes

$$\frac{R_0\,d\theta\,dx}{4\pi s_d^3}(R_0-r_j\cos\theta) \tag{A2}$$

where $s_d = (R_0^2+r_j^2+s^2-2R_0r_j\cos\theta)^{1/2}$ and $s = x-x_i$. Hence, the angle factor from the elementary gas volume $r_j\,dr\,d\theta\,dx$ to the elementary ring area $R_0\,dx(2\pi)$ on the torch wall at (R_0, x) can be calculated by

$$\frac{R_0\,dx}{4\pi}2\int_0^x\frac{(R_0-r_j\cos\theta)\,d\theta}{(R_0^2+r_j^2+s^2-2R_0r_j\cos\theta)^{3/2}}. \tag{A3}$$

Due to the axisymmetry of the plasma torch, (A3) is applicable to any elementary gas volume with coordinates (r_j, x_i) and is independent of azimuthal angle θ. Hence, the radiative heat flux contribution due to the elementary volume of the gas ring $2\pi r_j\,dr\,dx$ at the position (r_j, x_i) to the elementary ring area $2\pi R_0\,dx$ at the location (R_0, x) is

$$d(q_{w,s})_{ij} = \frac{U_t r_j\,dr\,dx}{2\pi R_0^2}$$
$$\times\int_0^x\frac{[1-(r_j/R_0)\cos\theta]\,d\theta}{\left[1+\left(\frac{r_j}{R_0}\right)^2+\left(\frac{x-x_i}{R_0}\right)^2-2\left(\frac{r_j}{R_0}\right)\cos\theta\right]^{3/2}}. \tag{A4}$$

It is easy to obtain equation (42) from equation (A4).

Equation (A4) is somewhat different from the similar expression obtained in ref. [19], in which the factor $\sin\phi'$ in (A1) was omitted.

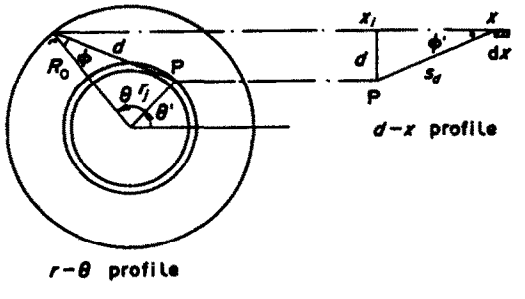

FIG. A1. Profiles showing the geometric parameters for the derivation of the radiative heat flux.

ECOULEMENT ET TRANSFERT THERMIQUE DANS UNE TORCHE A PLASMA A FREQUENCE RADIO—UNE NOUVELLE MODELISATION

Résumé—Une modélisation bidimensionnelle incluant une formulation de champ électromagnétique (EM) bidimensionnelle est décrite pour prédire l'écoulement et le transfert thermique de plasma à fréquence radio dans lesquels l'écoulement et le transfert thermique sont fortement couplés avec le champ EM. Les lignes de courant et les isothermes calculées sont présentées pour différents niveaux de puissance de la torche et elles sont comparées avec celles obtenues par une approche antérieure. Quelques résultats de calculs sont ajoutés pour des conditions thermiques plus compliquées à la paroi et concernant le flux radiatif sur la paroi.

EIN NEUES VERFAHREN ZUR BERECHNUNG VON WÄRMETRANSPORT UND STRÖMUNG IN EINER PLASMAFLAMME BEI RADIOFREQUENZ

Zusammenfassung—In dieser Arbeit wird ein vollständig zweidimensionales Verfahren zur Berechnung von Strömung und Wärmetransport in einer Plasmaflamme bei Radiofrequenz vorgestellt. Das Modell enthält eine Beschreibung des zweidimensionalen selbsterhaltenden elektromagnetischen Feldes, das stark mit der Strömung und dem Wärmetransport gekoppelt ist. Für unterschiedliche Flammleistungen werden berechnete Stromlinien- und Isothermenverläufe vorgestellt und mit früheren Berechnungen verglichen. Außerdem werden Rechenergebnisse für kompliziertere Wärmeübergangsbedingungen an der Wand mitgeteilt, dabei wird u.a. der Strahlungswärmeaustausch an der Wand berücksichtigt.

НОВЫЙ ПОДХОД К МОДЕЛИРОВАНИЮ ТЕПЛОПЕРЕНОСА И ТЕЧЕНИЯ В ВЫСОКОЧАСТОТНОЙ ПЛАЗМЕННОЙ ГОРЕЛКЕ

Аннотация—Описывается двумерная модель расчета течения плазмы и теплопереноса в радиочастотных плазменных горелках, в которых течение и теплоперенос сильно связаны с ЭМ полями, учитывающая влияние двумерного самосогсолаванного ЭМ поля. Представлены рассчитанные контуры линий тока и температур для различных уровней мощности горелки. И проведено их сравнение с результатами предыдущего подхода. Представлены некоторые дополнительные расчетные результаты для более сложного теплопереноса на стенке горелки, учитывающие радиационный тепловой поток вдоль стенки.